ECCOMAS Congress 2016
VII European Congress on Computational Methods in Applied Sciences and Engineering
M. Papadrakakis, V. Papadopoulos, G. Stefanou, V. Plevris (eds.)
Crete Island, Greece, 5–10 June 2016

A 3D ISOGEOMETRICAL BOUNDARY ELEMENT ANALYSIS FOR NONLINEAR GRAVITY WAVE PROPAGATION

Jorge Maestre[1], **Jordi Pallarés**[1], **Ildefonso Cuesta**[1]

[1]Departament d'Enginyeria Mecànica, Universitat Rovira i Virgili, Av. Països Catalans, 26, 43007 Tarragona, Spain.
{jorge.maestre,jordi.pallares,ildefonso.cuesta}@urv.cat

Keywords: BEM, T-spline, NURBS, Gravity wave, Time domain, non-linear waves

Abstract. *In this paper we describe a three-dimensional Isogeometric BEM in the time domain based on the T-spline and Non Uniform Rational B-Splines (NURBS) basis to study the free surface behavior. Traditionally, the Lagrange polynomials have been used to discretize the geometry and the BEMs variables. The Lagrange basis are discontinues across the elements although the physical variables are continuous. In dynamics problems with high mesh distortions this approach can produce numerical instabilities that can be quickly propagated. This problem could be overcome using T-spline or NURB basis. The main advantages of this approach are: (1) the control of the continuity and smoothness of the T-spline and NURBS basis, which makes the model numerically stable without the need of artificial smooth techniques;(2) the high order geometrical approximation by non-rational splines;(3) the refinement capabilities without affecting the geometry and BEM's variables; and (4) the direct integration with computer aid geometrical design tools. We use the concept of the Bézier extraction operation which provides an element point of view of the T-Spline and NURBS similar to the traditional finite element. The boundary integral Equation is solved at each time step by the GMRES algorithm and the time marching scheme is performed with a fourth-order Runge-Kutta method to update the model. Additionally, the hydrodynamic force is calculated by an auxiliary boundary equation. Some numerical benchmark examples are analysed to show the accuracy and the stability of the method*

1 INTRODUCTION

In the last decades, numerical models have been developed for the prediction of the propagation of gravity waves in the time domain. These models have been applied to simulated tsunami generation and [1] overturning waves [2–4], to design breakwaters [5, 6], to predict the wave pressure impact on structures [7], or to study radiation and diffraction waves produced by a wave-maker [8–11]. Nowadays, because of the increasing interest on the ocean renewable energy, in which the generation systems are installed near-shore or off-shore, new applications of such models are being used to study the fluid-structure interaction considering the effect of the waves [12–16].

Early numerical studies on the non-linear wave propagation appeared in 1976 when Longuet-Higguin and Cokelet [17] presented their bi-dimensional (2D) approach to simulate the transient surface waves. Their approach was based on the potential flow theory and used the Boundary Element Method (BEM) to solve the Laplace's equation in conjunction with a Mixed Eulerian-Lagrange (MEL) technique to update the free surface. Similar models were used to study a wide variety of non-linear water waves problems [18–22], but it was the study of Dommermuth et al. [23] that demonstrated the validity of the potential flow theory applied to the unsteady gravity wave propagation. These authors presented a successful comparison between the numerical results obtained by a 2D-BEM model and experimental results in a water tank. It is worth to mention the studies reported by Grilli et al. [2, 24, 25] who developed an advanced approach using 2D high order BEM. Later, Grilli et al. [3] and Guyenne and Grilli [4] extended the model to three-dimensional (3D) geometries to analyse overturning waves over an arbitrary bottom.

Some full non-linear high-order 3D BEM models have been proposed to simulate the unsteady interaction of the wave with a rigid body. An overview of such works can be found in Tanizawa [26]. Among them, Lee et al. [27] studied the non-linear waves and the hydrodynamic force generated by the movement of a submerged sphere. Bai and Taylor [10] investigated the wave radiation produced by a moving submerged truncated cylinder and the wave diffraction around a vertical cylinder [28]. They used an unstructured triangular mesh constructed with second order Lagrange elements in order to obtain a good approximation of the geometry. Later, these authors extended the model to flared floating structures [29]. Sung and Grilli [30] analysed the waves generated by an advancing surface disturbance. Following the Grilli's works, these authors used a structured mesh formed by isoparametric bi-cubic piecewise overlapping elements that provided a local smoothness of the geometry and of the physical variables. More recently, Hannan et al. [31, 32] studied the interactions between water waves and fully submerged fixed or moving structures. In the same line, but limited to 2D, Dombre et al. [33] extended the early work presented in [34] to study the dynamics of free fully submerged structures.

In addition, other models have been proposed to analyse more specific problems such as the post-breaking phenomenon, violent wave impact against structures, large fluid movement in confined space with steep non-linear waves or viscous and vortex force in the context of floating structure. In such cases, the potential flow theory is not valid and other tools based on Computational Fluid Dynamics (CFD) solvers to resolve the full Navier-Stokes equations or Lattice Boltzmann method (LBM) have been used [35–40]. Most of these problems have been formulated in 2D, and despite the increase of computational power, the full 3D models require a considerable computational cost. Therefore, unless in such specific cases, the potential theory together with BEM provides good results for non-linear gravity waves problems with reduced computational time. Some advantages are: (1) the reduced dimensionality of the domain; (2)

the ability to handle complex 3D geometric models; (3) and the Sommerfeld radiation condition is implicitly satisfied in the Green function.

In the last two decades, the Non-Uniform Rational B-Spline (NURBS) representation has been widely used in the marine industry through of the modern Computational Aid Design (CAD) systems. NURBS exhibits multiple advantages, such as: (1) the quadratic surface can be represented exactly; (2) advanced construction techniques and shape modification tools are available (3) the smoothness of the basis can be managed via knot; and (4) h, p and k-refinement can be applied without modifying the geometry. These characteristics, in combination with other mathematical properties, give to NURBS the ability to handle complex geometries and provide suitable basis for numerical analyses. In this line, the incorporation of NURBS into the BEM to simulate wave-structure interaction has appeared recently in the literature (see for example references [41–46]). These approaches use two different basis functions, one to represent the geometry and the other for physical variables. Hughes et al. [47, 48] and Cottrell et al. [49, 50] introduced the concept of the Isogeometrical Analysis (IGA) in the context of Finite Element Method (FEM) that consists on approximate the full model by the same basis functions used for the geometry. This concept, that has acquired enough maturity in recent years, allows a direct link between the CAD geometry and the engineering analysis tools. Politis et al. [51] extended the IGA to the BEM and applied it to a 2D external potential flow problem. Simpson et al. [52] applied an IGA-BEM method to a 2D elastoestatic problem. More recently, Belibassakis et al. [53] presented a 3D IGA-BEM model based on the Neumann-Kelvin problem to study the ship wave resistance and showed a novel combination of a modern CAD system with hydrodynamic solvers.

Although the NURBS is widely used by the CAD industry, it has some limitations associated with the fact that only surfaces with four edges can be represented. This entails that complicated geometries require many NURBS patches and the smoothness between patches is lost. The T-spline technology has been introduced to overcome these limitations [54]. T-splines are a generalization of the NURBS, in which several NURBS patches can be integrated into a unique T-spline. Moreover, unlike the NURBS, T-splines allow local refinements and unstructured meshes this makes their use attractive for the engineering analyses. In this direction, Scott et al. [55] and Li et al. [56] formulated the analysis-suitable T-spline in which necessary mathematical properties of the basis (as linear independence) are guaranteed to be used in IGA. However, the implementation of T-spline in the IGA requires a more advanced development. Adopting the idea of the Bézier extraction operation, presented by Borden et al. [57] and Scott et al. [58], the T-spline and NURBS can be incorporated efficiently via modifying the shape functions in the classical BEM and FEM. Thomas et al. [59] developed a generalization of such technique. In recent years, the application of the T-spline in the IGA framework to different areas has been developed [60–64]. In the context of IGA-BEM Scott et al. [58] extended the analysis-suitable T-spline to unstructured meshes for elastostatic problems and developed a collocation procedure based on a generalization of the Grenville abscissae. Simpson et al. [65] applied this method to acoustic problems and demonstrated the higher accuracy in comparison to the conventional Lagrange discretization due to the superior geometric approximation. Ginnis et al. [66] exploited IGA-BEM based on the T-spline to analyse in the ship wave resistance problem and Kostas et al. [67] used this method to optimize the hull shape.

Other alternatives to analysis-suitable T-spline are appearing in the literature. These alternatives include hierarchical spline (B-splines, NURBS and T-spline), PHT-splines and LR-splines. In addition to the limited works cited above, the interested reader can be found an overview of the IGA [68].

The literature review performed shows that the IGA-BEM based on the NURBS and analysis-suitable T-spline reveals that is a very recent topic. The objective of this study is the application of this method to solve non-linear unsteady gravity wave propagation and wave-structure interaction problems. We consider the full non-linear potential flow theory in combination with the MEL procedure. In this work we exploit the advantages of the IGA-BEM based on T-spline and NURBS basis in the framework of the Bézier extraction procedure. The high continuity of the basis functions allows to deal with large mesh distortion [69] in the Lagrange formulation as well as it prevents numerical instabilities as the saw-tooth effect that occurs when classical C^0 piecewise basis are used. The Bézier extraction concept provides an easy and standard way to introduce the NURBS and T-spline basis in the BEM. In addition, we employ direct integration with CAD software [70] to make and handle 3D geometrical models.

2 FORMULATION OF THE PROBLEM

We consider a fluid volume $\Omega(t)$ defined by an arbitrary lateral boundary $\Gamma_W(t)$, composed by one or several surfaces, a bottom surface $\Gamma_S(t)$ and a free surface $\Gamma_F(t)$ located at the top. The fluid can move freely with the time (t) by the action of a submerged moving rigid body $\Gamma_B(t)$ or by imposing a specific initial condition. In Fig. 1 we show a sketch of the domain and the Cartesian coordinate adopted. The plane $z = 0$ corresponds to the free surface at rest.

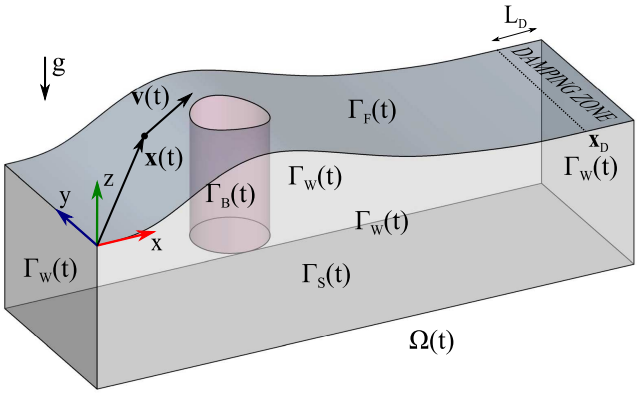

Figure 1: Sketch of the problem

The flow is assumed to be incompressible, inviscid and irrotational fluid. Under these hypotheses, the movement of a fluid particle $\mathbf{x}(t)$ can be described in terms of a velocity potential $(\phi(x, y, z, t))$, such that the velocity of a fluid particle can be expressed as:

$$\mathbf{v} = \boldsymbol{\nabla}\phi \tag{1}$$

The continuity equation in the a fluid domain $\Omega(t)$ can be reduced to a Laplace equation:

$$\nabla^2\phi = 0 \qquad \text{in } \Omega(t) \tag{2}$$

that is subjected to different boundary conditions on the surfaces $\Gamma(t)$ that define the domain.

On the free surface $\Gamma_F(t)$, the kinematic and dynamic conditions in the Lagrangian descrip-

tion are expressed as:

$$\frac{D\mathbf{x}}{Dt} = \boldsymbol{\nabla}\phi \qquad \text{on } \Gamma_F(t) \tag{3}$$

$$\frac{D\phi}{Dt} = -gz + \frac{1}{2}\boldsymbol{\nabla}\phi \cdot \boldsymbol{\nabla}\phi - \frac{p_a}{\rho} \qquad \text{on } \Gamma_F(t) \tag{4}$$

respectively. In Eqs. (3-4) D/Dt denotes the material derivative, g is the gravity acceleration, p_a is the atmospheric pressure and ρ is the density of the fluid.

The instantaneous kinematic conditions on the lateral boundaries $\Gamma_W(t)$, the bottom $\Gamma_S(t)$ and wetted body surfaces $\Gamma_B(t)$ are:

$$\frac{\partial\phi}{\partial n} = 0 \qquad \text{on } \Gamma_W(t) \text{ and } \Gamma_S(t) \tag{5}$$

$$\frac{\partial\phi}{\partial n} = \mathbf{v}_B \cdot \mathbf{n} \qquad \text{on } \Gamma_B(t) \tag{6}$$

with $\mathbf{n}$ the normal pointing out of fluid and $\mathbf{v}_B$ the velocity vector of the rigid body. In the case of a free floating body, the velocity should be computed using the second Newton's law. Here we consider the rigid body motion given by $\mathbf{v}_B = \dot{\mathbf{x}}_G + \dot{\boldsymbol{\theta}}_G \times \mathbf{r}_B$, where $\dot{\mathbf{x}}_G$ and $\dot{\boldsymbol{\theta}}_G$ are the velocity and rotation vectors referred to the center of mass, and $\mathbf{r}_B = \mathbf{x}_B - \mathbf{x}_G$ is the location of a body particle respect to the center of mass.

As it can be noted in the formulation expressed above, the lateral boundaries are considered solid and impermeable. This means that waves are reflected and kept into the domain as it would occur in a tank. In some cases treated in this study, we are interested on simulating an infinite domain. For these cases, an artificial damping method is used to absorb the wave energy near the boundaries [10, 71]. This is done by modifying the kinematic and dynamic boundary conditions over a finite zone of the free surface, known as damping zone, located near the boundaries as follows:

$$\frac{D\mathbf{x}}{Dt} = \boldsymbol{\nabla}\phi - \mu(\mathbf{x})(\mathbf{x} - \mathbf{x}_0) \qquad \text{on } \Gamma_F(t) \tag{7}$$

$$\frac{D\phi}{Dt} = -gz + \frac{1}{2}\boldsymbol{\nabla}\phi \cdot \boldsymbol{\nabla}\phi - \frac{p_a}{\rho} - \mu(\mathbf{x})(\phi - \phi_0) \qquad \text{on } \Gamma_F(t) \tag{8}$$

where $\mathbf{x}_0$ and ϕ_0 are reference values at the rest state, and $\mu(\mathbf{x})$ is the damping factor, which is gradually increasing along the damping zone as:

$$\mu(\mathbf{x}) = \begin{cases} \alpha \left(\frac{l_D(\mathbf{x})}{L_D}\right)^2 & \text{in damping zone} \\ 0 & \text{otherwise} \end{cases} \tag{9}$$

In Eq. 9 α is the maximum damping factor, L_D is the length of the zone and $l_D(\mathbf{x})$ is distance between $\mathbf{x}_D$ and the specific location considered (see Fig. 1).

3 FORMULATION OF THE METHOD

3.1 Geometry

Considering a 3D BEM model, the geometry of the problem is defined uniquely by the boundary surfaces Γ of the fluid domain. In this paper we use NURBS and cubic T-spline technology which are widely used in CAD applications. Particularly, we focus on 3D surfaces

where the physical space is given by $\Gamma \in \Re^{d_s}$ with $d_s = 3$ and the parameter space can be reduced to $\widehat{\Gamma} \in \Re^{d_p}$ with $d_p = 2$.

A NURBS surface is described in terms of a control mesh and a valid pair of knot vectors. A knot vector is denoted by $\Xi^i = \{\xi_1^i, \xi_2^i, ..., \xi_{1+n_i+p_i}^i\}$, where $\xi_k^i \in \Re$ is the kth knot value, and n_i is the number of B-spline basis functions of degree p_i in the i direction. Hereinafter, we denote the multi-index $\mathbf{p} = \{p_1, p_2\}$, $\mathbf{n} = \{n_1, n_2\}$ and the parametric coordinate $\boldsymbol{\xi} = \{\xi^1, \xi^2\}$. The control mesh is a set of vertices that forms a structured set of quadrilateral elements. Each vertex has associated a control point $\mathbf{P}_A \in \Re^{d_s}$ and a weight $w_A \in \Re$, where $A = 1, 2, ..., n_{cp}$ is the global index that denotes all vertices $n_{cp} = \prod_{i=1}^{d_p} n_i$.

If we define the parametric space by $\widehat{\Gamma} = [\xi_1^1, \xi_{1+n_1+p_1}^1] \times [\xi_1^2, \xi_{1+n_2+p_2}^2]$, the NURBS surface that maps the parametric space to the physical space $\mathbf{x} : \widehat{\Gamma} \rightarrow \Gamma$ can be expressed as:

$$\mathbf{x}(\boldsymbol{\xi}) = \frac{\sum_{A=1}^{n_{cp}} \mathbf{P}_A w_A N_A(\boldsymbol{\xi})}{\sum_{A=1}^{n_{cp}} w_A N_A(\boldsymbol{\xi})} = \sum_{A=1}^{n_{cp}} \mathbf{P}_A R_A(\boldsymbol{\xi}) \qquad \boldsymbol{\xi} \in \widehat{\Gamma} \tag{10}$$

where $N_A(\boldsymbol{\xi})$ is the bivariate B-spline basis functions associated with the global vertex A and $R_A(\boldsymbol{\xi})$ denotes the rational basis functions made by the weights and the B-spline basis functions.

Note that the NURBS is limited to surfaces defined by four edges. To represent more complex geometries it is necessary to divide the models in different rectangular patches. This limitation can be overcome naturally using the T-spline framework T-splines which allows the existence of hanging and extraordinary points within the control mesh. For a cubic T-spline, the mapping is expressed in a similar way as in Eq. (10). However, unlike NURBS, the surface is locally parametrized by defining of a local pair of knot interval vectors $\Delta\Xi_A^i = \{\Delta\xi_{A,1}^i, \Delta\xi_{A,2}^i, ..., \Delta\xi_{A,1+p_i}^i\}$ with $\Delta\xi_i = \xi_{i+1} - \xi_i$, associated to each vertex A where the T-spline basis functions is restricted to be non-null. This provides the capacity of making unstructured meshes and local refinements. For more details about the T-spline or NURBS theory, the reader is refereed to [47, 55, 72–75].

3.2 A finite element structure

The idea is to discretize the physical domain with a series of independent elements $\mathbf{x}^e(\tilde{\boldsymbol{\xi}})$ defined over a parent domain $\tilde{\boldsymbol{\xi}} \in \widetilde{\Gamma}$ [57]. Considering the compact support property of the basis functions, there exists a number of them, n_e, which are non-null over each element e. Then, we can construct a matrix $A = IEN(e, a)$, that maps the local basis functions number a in the element e to the global function A. The local geometry, restricted to each element domain, is defined as:

$$\mathbf{x}^e(\tilde{\boldsymbol{\xi}}) = \frac{\sum_{a=1}^{n_e} \mathbf{P}_a^e w_a^e N_a^e(\tilde{\boldsymbol{\xi}})}{\sum_{a=1}^{n_e} w_a^e N_a^e(\tilde{\boldsymbol{\xi}})} \qquad \tilde{\boldsymbol{\xi}} \in \widetilde{\Gamma} \tag{11}$$

and in compact form it can be rewritten as:

$$\mathbf{x}^e(\tilde{\boldsymbol{\xi}}) = \frac{(\mathbf{P}^e)^T \mathbf{W}^e \mathbf{N}^e(\tilde{\boldsymbol{\xi}})}{\mathbf{w}^e \mathbf{N}^e(\tilde{\boldsymbol{\xi}})} \qquad \tilde{\boldsymbol{\xi}} \in \widetilde{\Gamma} \tag{12}$$

where $\mathbf{P}^e = \{\mathbf{P}_a^e\}_{a=1}^{n_e}$ is a set of the control points, $\mathbf{w}^e = \{W_a^e\}_{a=1}^{n_e}$ is a vector of weights, $\mathbf{W}^e = diag(\mathbf{w}^e)$ is a diagonal matrix and $\mathbf{N}^e(\tilde{\boldsymbol{\xi}}) = \{N_a^e(\tilde{\boldsymbol{\xi}})\}_{a=1}^{n_e}$ is a vector of the basis functions relative to the element e.

It should be noted that the number of T-spline basis functions contained in each element can be different, while in the case of NURBS are exactly equal to $\prod_{i=1}^{d_p}(p_i + 1)$. Furthermore, the

T-spline and NURBS basis functions affect to different elements and their definition depends on the topology. An elegant and efficient way to standardize the T-spline and NURBS basis functions to the same set of compact basis functions restricted to a unique element is using the Bézier extraction operator. This operator determines the Berstein basis combination ($B_{\mathbf{p}}(\tilde{\boldsymbol{\xi}})$ of $\mathbf{p}$ degree) in which the T-spline and NURBS basis functions are decomposed.

Let us define a vector of the Berstein basis functions $\mathbf{B}(\tilde{\boldsymbol{\xi}}) = \{B_{a,\mathbf{p}}(\tilde{\boldsymbol{\xi}})\}_{a=1}^{n_B}$ with $n_B = \prod_{i=1}^{d_p}(p_i+1)$. The geometry, can be expressed as:

$$\mathbf{x}^e(\tilde{\boldsymbol{\xi}}) = \frac{(\mathbf{P}^e)^T\mathbf{W}^e\mathbf{C}^e\mathbf{B}^e(\tilde{\boldsymbol{\xi}})}{\mathbf{w}^e\mathbf{W}^e\mathbf{C}^e\mathbf{B}^e(\tilde{\boldsymbol{\xi}})} = (\mathbf{P}^e)^T\mathbf{R}^e(\tilde{\boldsymbol{\xi}}) \qquad \tilde{\boldsymbol{\xi}} \in \widetilde{\Gamma} \tag{13}$$

being $\mathbf{C}^e \in \Re^{n_e \times n_B}$ the matrix extractor operator corresponding to the element e that only depends on the topology. This method provides a Bézier-element point of view such that the geometry is decomposed in a set of Bézier elements without changing the properties of the geometry. In addition, this method provides a equivalent treatment for T-spline and NURBS. A detailed explanation of the Bézier extraction can be found in [57–59].

3.3 Isogeometric BEM

Given the domain $\Omega(t)$ delimited for a piecewise smooth boundary $\Gamma(t)$, the external Boundary Integral Equation (BIE) applied to the potential problem can be written as:

$$C(\mathbf{x}_0)\phi(\mathbf{x}_0,t) = \int_{\Gamma(t)} \left[G(\mathbf{x},\mathbf{x}_0)\frac{\partial\phi(\mathbf{x},t)}{\partial n} \right] d\Gamma - \fint_{\Gamma(t)} \left[\phi(\mathbf{x},t)\frac{\partial G(\mathbf{x},\mathbf{x}_0)}{\partial n} \right] d\Gamma \tag{14}$$

The symbol $\fint$ denotes that the integral is evaluated in the Cauchy Principal Value sense, $C(\mathbf{x}_0)$ is the solid angle defined at the source point $\mathbf{x}_0 \in \Gamma$, that can be calculated directly with the expression proposed by Mantic [76] or indirectly as described in Section 4.1, and $G(\mathbf{x},\mathbf{x}_0)$ is the fundamental solution of the Laplace's problem. In the examples treated here, we consider three possible orthogonal symmetric planes parallel to the Cartesian planes, such that the geometric complexity and computational costs can be reduced. Using the method of the images, the Green function can be expressed as:

$$G(\mathbf{x},\mathbf{x}_0) = \frac{-1}{4\pi}\sum_{i=1}^{8}\left[\frac{1}{\|\mathbf{x}-\mathbf{x}\prime_i\|}\right] \tag{15}$$

where:

$$\begin{cases} \mathbf{x}\prime_1 = \mathbf{x}_0 \\ \mathbf{x}\prime_2 = \{x_0, y_0, 2z_{sym} - z_0\} \\ \mathbf{x}\prime_3 = \{x_0, 2y_{sym} - y_0, z_0\} \\ \mathbf{x}\prime_4 = \{x_0, 2y_{sym} - y_0, 2z_{sym} - z_0\} \\ \mathbf{x}\prime_5 = \{2x_{sym} - x_0, y_0, z_0\} \\ \mathbf{x}\prime_6 = \{2x_{sym} - x_0, y_0, 2z_{sym} - z_0\} \\ \mathbf{x}\prime_7 = \{2x_{sym} - x_0, 2y_{sym} - y_0, z_0\} \\ \mathbf{x}\prime_8 = \{2x_{sym} - x_0, 2y_{sym} - y_0, 2z_{sym} - z_0\} \end{cases} \tag{16}$$

with $x = x_{sym}$, $y = y_{sym}$ and $z = z_{sym}$ being the location of the symmetric planes.

Considering a Isogeometric Analysis (IGA), the variables introduced in the BIE (i.e. the potential and the flux) are defined in a finite dimensional space given by the same basis functions

than the geometry. This provides the BIE variables and the geometry the intrinsic properties of the T-spline (or NURBS) as demonstrated in the previous section. The BIE variables can be written as:

$$\phi^e(\tilde{\boldsymbol{\xi}}, t) = \mathbf{R}^e(\tilde{\boldsymbol{\xi}})^T \boldsymbol{\phi}^e(t) \tag{17}$$

$$\frac{\partial \phi^e}{\partial n}(\tilde{\boldsymbol{\xi}}, t) = q^e(\tilde{\boldsymbol{\xi}}, t) = \mathbf{R}^e(\tilde{\boldsymbol{\xi}})^T \boldsymbol{q}^e(t) \tag{18}$$

where $\boldsymbol{\phi}^e(t) = \{\phi_a^e(t)\}_{a=1}^{n_e}$ and $\boldsymbol{q}^e(t) = \{q_a^e(t)\}_{a=1}^{n_e}$ are the temporal potential and temporal flux vector corresponding to the local basis functions of each element, respectively.

Introducing Eqs. (17) and (13) into Eq. (14), and applying the result on a particular source point $\mathbf{x}_i^{e_i} = \mathbf{R}_i^{e_i}(\tilde{\boldsymbol{\xi}}_i^{e_i})^T \mathbf{P}^{e_i}$ contained in the element e_i, we obtain the discrete IGA BIE:

$$C(\mathbf{x}_i^{e_i})(\mathbf{R}_i^{e_i})^T \boldsymbol{\phi}^{e_i} = \sum_{e=1}^{N} \left[\int_{\Gamma^e(t)} \left[G(\mathbf{x}^e, \mathbf{x}_i^{e_i})(\mathbf{R}^e)^T \boldsymbol{q}^e \right] \left| \frac{\partial \mathbf{x}^e}{\partial \tilde{\boldsymbol{\xi}}} \right| d\Gamma(\tilde{\boldsymbol{\xi}}) \right.$$
$$\left. - \cancel{\int}_{\Gamma^e(t)} \left[(\mathbf{R}^e)^T \boldsymbol{\phi}^e \frac{\partial G(\mathbf{x}^e, \mathbf{x}_i^{e_i})}{\partial n} \right] \left| \frac{\partial \mathbf{x}^e}{\partial \tilde{\boldsymbol{\xi}}} \right| d\Gamma(\tilde{\boldsymbol{\xi}}) \right] \tag{19}$$

In Eq. (19) $\left| \frac{\partial \mathbf{x}^e}{\partial \tilde{\boldsymbol{\xi}}} \right|$ is the Jacobian determinant of the geometrical mapping, N is the number of elements. For more details about the calculation of the Jacobian and the tangential derivatives, the reader is referred to [57, 77]. Hereinafter, we drop the upper index e_i and for convenience we keep the subindex i to refer to the source point.

In this study we employ a collocational method, such that the BIE must be satisfied for a set of $i = 1, 2, ..., n_{cp}$ specific source points known as collocation points. Particularly, we use a generalization of the Greville abscissae as presented in Scott et al. [58], since it provides accurate results in the context of the IGA BEM. However, we relax the continuity condition for the position of control points such as these are allowed to lie in sharp edges and corners. As demonstrated in [65], this relaxation does not reduce the accuracy of the results and it facilitates the special treatment of the velocity in these locations, as shown in Section 4.3.

4 NUMERICAL IMPLEMENTATION

4.1 Numerical integration

It is well known that the first and second kernel of the BIE (see Eq. 14) contain a weak and a strong singularity, respectively, when the point of evaluation approaches to the collocation point. The integrals are defined, but they have to be suitably evaluated to avoid numerical problems. This topic has been studied intensively and an overview of the available techniques can be found in [78–87].

In this study we regularize the second kernel using the rigid body method [78], that provides an indirect way to calculate the jump term as:

$$C(\mathbf{x}_0) = -\cancel{\int}_{\Gamma(t)} \frac{\partial G(\mathbf{x}, \mathbf{x}_0)}{\partial n} d\Gamma \tag{20}$$

Introducing Eq. 20 in Eq. 14 gives:

$$\int_{\Gamma(t)} \left[(\phi(\mathbf{x}, t) - \phi(\mathbf{x}_0, t)) \frac{\partial G(\mathbf{x}, \mathbf{x}_0)}{\partial n} \right] d\Gamma = \int_{\Gamma(t)} \left[G(\mathbf{x}, \mathbf{x}_0) \frac{\partial \phi(\mathbf{x}, t)}{\partial n} \right] d\Gamma \tag{21}$$

The weak singularity is solved using a local change of variables over the element containing the collocation point, as proposed by Lachat and Watson [79]. Once regularized, these kernels can be numerically evaluated by applying the quadrature rule to each element in the parent domain. We use the standard Gauss-Legendre quadrature. Recently, new specific quadrature rules for NURBS have been proposed to take into account the continuity of the basis functions [80]. In addition, if the collocation point is not located on the element but very close, the integrals become nearly singular and their calculation can exhibit numerical instability. For this case, we use an adaptive regular element subdivision on the parent domain.

4.2 System of equations

The discretization of the BIE in all collocation points leads to a set of n_{cp} equations with $2n_{cp}$ variables corresponding to the potential and the flux at the control points. This set of equations can be written compactly as,

$$(\mathbf{C}\boldsymbol{\mathcal{T}} + \boldsymbol{\mathcal{H}})\,\boldsymbol{\phi} = \boldsymbol{\mathcal{G}}\mathbf{q} \tag{22}$$

in which, using the global notation, $\boldsymbol{\phi} = \{\phi\}_{A=1}^{n_{cp}}$ is the potential vector, $\mathbf{q} = \{q\}_{A=1}^{n_{cp}}$ is the flux vector, and the matrices $\mathbf{C}$, $\boldsymbol{\mathcal{T}}$, $\boldsymbol{\mathcal{H}}$ and $\boldsymbol{\mathcal{G}} \in \Re^{n_{cp}\times n_{cp}}$ are given by:

$$\boldsymbol{\mathcal{H}}_{iA} = \int_{\Gamma(t)} \frac{\partial G(\mathbf{x}, \mathbf{x}_i)}{\partial n} R_A d\Gamma \tag{23}$$

$$\boldsymbol{\mathcal{G}}_{iA} = \int_{\Gamma(t)} G(\mathbf{x}, \mathbf{x}_i) R_A d\Gamma \tag{24}$$

$$\boldsymbol{\mathcal{T}}_{iA} = R_A(\mathbf{x}_i) \tag{25}$$

$$\mathbf{C}_{iA} = -\delta_{iA} \sum_{k=1}^{n_{cp}} \boldsymbol{\mathcal{H}}_{ik} \tag{26}$$

As it has been shown in Section 2, the problem under consideration consists in a mixed boundary problem in which the potential, once integrated in time, is known on the free surface and its flux on the rest of the boundaries. The discretization of the boundary conditions on the set of collocation points yields,

$$\mathbf{R}(\mathbf{x}_i)^T \boldsymbol{\phi} = \bar{\phi}(\mathbf{x}_i) \qquad \forall \mathbf{x}_i \in \Gamma_F(t) \tag{27}$$

$$\mathbf{R}(\mathbf{x}_i)^T \mathbf{q} = \bar{q}(\mathbf{x}_i) \qquad \forall \mathbf{x}_i \in \Gamma_W(t) \cup \Gamma_S(t) \cup \Gamma_B(t) \tag{28}$$

We reorder the system of equations (22), (27) and (28) to obtain a linear system that can be written as $\mathbf{Ka} = \mathbf{b}$, where $\mathbf{a} \in \Re^{2n_{cp}}$ is a vector containing the control variables, $\mathbf{b} \in \Re^{2n_{cp}}$ is a vector with the boundary conditions at the collocation points and $\mathbf{K} \in \Re^{2n_{cp}\times 2n_{cp}}$ is in general a dense non-symmetric matrix. The minimum residual method (GMRES) have been found to be efficient and suitable for solving the system of equations [10, 88]. In the present study the tolerance has been set to 10^{-12}. Moreover, to correctly model the physical variables at the sharp edge and corners, we use the semi-discontinuous basis technique, as presented in [58], such that the flux is allowed to be discontinuous while the potential is continuous.

4.3 Velocity field

Before the update of the free surface, we need to calculate the velocity field. Following the idea of IGA, we use the same set of T-spline (or NURBS) basis functions to approximate the

velocity which can be expressed as,

$$\mathbf{v}(\tilde{\boldsymbol{\xi}}, t) = \mathbf{R}(\boldsymbol{\xi})^T \mathbf{v}(t) \tag{29}$$

where $\mathbf{v}(t) = \{\mathbf{v}_A(t)\}_{A=1}^{n_{cp}}$ is the global velocity vector.

Using Eq. (1), the velocity of the fluid particle at any point of the domain can be determined as a function of the potential, of the flux and of the Jacobian of the mapping:

$$\begin{bmatrix} v_x \\ v_y \\ v_z \end{bmatrix} = \begin{bmatrix} \frac{\partial x}{\partial \xi^1} & \frac{\partial y}{\partial \xi^1} & \frac{\partial z}{\partial \xi^1} \\ \frac{\partial x}{\partial \xi^2} & \frac{\partial y}{\partial \xi^2} & \frac{\partial z}{\partial \xi^2} \\ n_x & n_y & n_z \end{bmatrix}^{-1} \begin{bmatrix} \frac{\partial \phi}{\partial \xi^1} \\ \frac{\partial \phi}{\partial \xi^2} \\ \frac{\partial \phi}{\partial n} \end{bmatrix} \tag{30}$$

In the case of a damping zone on the free surface, the terms on the right hand side have to be corrected as shown in Eq. (7).

The sharp edges and corners where several surfaces meet need a special attention. Because the derivatives of the potential and the flux are discontinuous at the intersections, the velocity associated to each surface can be numerically different and also it can be incompatible with the movement of each boundary. An usual procedure to overcome this problem is, first compute an average velocity and second make a normal projection of the intersections on the new boundary position during the time marching [10]. In this work we employ an alternative procedure that consists on calculating an unique velocity compatible with the normal velocity of each surface. We consider two possible cases as shown in Fig. 2. The first one (Fig. 2a) correspond to a corner at the intersection of three surfaces. In this case, the velocity can be determined using the follow equation:

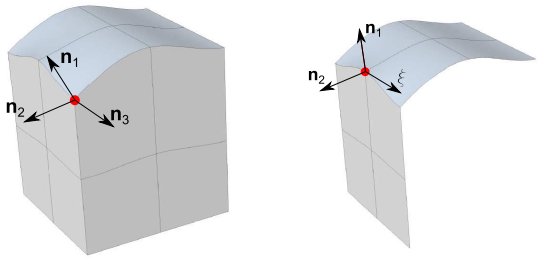

(a) (b)

Figure 2: (a) Corner at the intersection of three surfaces and (b) edge defined by the intersection two surfaces.

$$\begin{bmatrix} v_x \\ v_y \\ v_z \end{bmatrix} = \begin{bmatrix} n_x^1 & n_y^1 & n_z^1 \\ n_x^2 & n_y^2 & n_z^2 \\ n_x^3 & n_y^3 & n_z^3 \end{bmatrix}^{-1} \begin{bmatrix} \frac{\partial \phi}{\partial n^1} \\ \frac{\partial \phi}{\partial n^2} \\ \frac{\partial \phi}{\partial n^3} \end{bmatrix} \tag{31}$$

where n^i are the normals corresponding to each surface.

The second case (Fig. 2b) is found in the edge defined by the intersection of two surfaces. The velocity can be computed as,

$$\begin{bmatrix} v_x \\ v_y \\ v_z \end{bmatrix} = \begin{bmatrix} n_x^1 & n_y^1 & n_z^1 \\ n_x^2 & n_y^2 & n_z^2 \\ \frac{\partial x}{\partial \xi} & \frac{\partial y}{\partial \xi} & \frac{\partial z}{\partial \xi} \end{bmatrix}^{-1} \begin{bmatrix} \frac{\partial \phi}{\partial n^1} \\ \frac{\partial \phi}{\partial n^2} \\ \frac{\partial \phi}{\partial \xi} \end{bmatrix} \tag{32}$$

In Eq. (32) ξ represents the common axis along the direction of the edge. Note that, since ϕ is continuous, its derivative along the edge is unique.

Now, if we particularize Eq. (30) for the collocation points contained inside the surfaces, Eq. (32) for the collocation points on the edges and Eq. (31) for the corners, we obtain a system of equations (Eq. 33) that allows the determination of the global velocity vector.

$$\mathbf{v}(t) = \boldsymbol{\mathcal{T}}^{-1}\boldsymbol{\mathcal{V}} \tag{33}$$

In Eq. (33) $\boldsymbol{\mathcal{V}} = \{\mathbf{v}_i(\boldsymbol{\xi}_i, t)\}_{i=1}^{n_{cp}}$ is the velocity vector at the collocations points and $\boldsymbol{\mathcal{T}}$ is an invertible and well conditioned matrix. Note that this matrix, that we denote as the interpolation matrix, allows the mapping of the information of the control points to the collocation points. In addition, it can be applied to any variable because we use an IGA.

Therefore, using this procedure, the velocity field is forced to be unique and compatible with the normal movement of the body or the walls. Moreover, the intersections can be managed directly through collocation points due to the interpolatory nature of the basis functions at the sharp edges or corners. However, a slight separation of the intersections from the body or the walls can appear during the time marching. The points on these intersections are relocated back by the normal projection technique as proposed by Bai and Taylor [10].

4.4 Hydrodynamic pressure

The pressure force exerted by the fluid on the surface of a body can be computed as,

$$F_B = \int_{\Gamma_B(t)} p\mathbf{n} d\Gamma \tag{34}$$

The pressure field at any point can be calculated using the Bernoulli equation:

$$p = -\rho\left(\frac{\partial\phi}{\partial t} + gz + \frac{1}{2}\boldsymbol{\nabla}\phi\cdot\boldsymbol{\nabla}\phi\right) \tag{35}$$

The last term on the right hand side of the Eq. 35 can be computed directly once the BIE (14) is computed. The term $\frac{\partial\phi}{\partial t}$, which is not known at this stage, can be approximated by using temporal integration schemes. However, this can produce numerical errors. Here, we use an auxiliary BIE to find a more accurate approach. As proposed by Dombre et al. [3, 33], an analogous BIE for $\psi = \partial\phi/\partial t$ can be considered. This auxiliary BIE does not increase significantly the computational cost because the discretization is the same as in the main BIE. Only, the boundary conditions have to be changed. The equations for the new variable ψ can be written as,

$$\nabla^2\psi = 0 \qquad \text{in } \Omega(t) \tag{36}$$

$$\psi = -gz + \frac{1}{2}\boldsymbol{\nabla}\phi\cdot\boldsymbol{\nabla}\phi - \frac{p_a}{\rho} \qquad \text{on } \Gamma_F(t) \tag{37}$$

$$\frac{\partial\psi}{\partial n} = 0 \qquad \text{on } \Gamma_W(t) \text{ and } \Gamma_S(t) \tag{38}$$

$$\frac{\partial\psi}{\partial n} = \frac{d(\mathbf{v}_B\cdot\mathbf{n})}{dt} - (\mathbf{v}_B\cdot\boldsymbol{\nabla}\boldsymbol{\nabla}\phi)\cdot\mathbf{n} - \boldsymbol{\nabla}\phi\frac{d\mathbf{n}}{dt} \qquad \text{on } \Gamma_B(t) \tag{39}$$

where $\frac{d}{dt}$ denotes Lagrangian time derivative following the body motion.

4.5 Time marching

As shown in the formulation of the problem, the position of the fluid particles and the physical variables, Eq. (3) and Eq. (4), depend on the time. Therefore, to obtain the temporal evolution of the free surface, a temporal integration scheme is needed. In the context of strong non-linear gravity waves, several schemes has been proposed [3,29,71,90]. In this study, we use the the standard 4th order Runge Kutta method (RK4), which has been shown to be numerically stable and accurate.

An important aspect of temporal integration is the adequate selection of the time step to provide an accurate and stable temporal resolution. This depends on the integration scheme, physical discretization and the particular problem under consideration. For periodic wave problems the time step is usually chosen as a fraction of the wave period such that the physical phenomenon is represented accurately [71]. For a solitary wave, Grilli et al. [3] proposed an adaptive time steeping method as a function of the spatial discretization and the Courant number, $\mathcal{C}$ (Eq. 40). They demonstrated that there exists an optimal Courant number such that the error is minimum. We use this method, adapted to the IGA-BEM, and investigate about the optimal value of the Courant number.

$$\Delta t = \mathcal{C} Le_{min} / \sqrt{gh} \tag{40}$$

In Eq 40 Le_{min} is the minimum characteristic element size defined as the square root of its surface and h is the depth of the bottom surface.

The steps for the time marching procedure are:

1. The initial geometrical model is defined and an initial boundary condition for the potential ($\bar{\phi}_0$) and the flux ($\bar{q}_0$) are specified on the free surface and on the rest of the surfaces, respectively.

2. A time step (Δt_n) is selected. This can be set dynamically at each step depending on the type of problem.

3. The time integration is carried out to update the position of the fluid particles and potential (ϕ_{n+1}, $\mathbf{x}_{n+1}$) from the actual time (t_n) to the next time step ($t_{n+1} = t_n + \Delta t_n$). Due to the non-linear behaviour, several sub-steps are required.

- **3**.1. The BIE equation (22) is calculated, and the boundary conditions (Eq. (27) and Eq. (28)) are applied at the each sub-step (k). A linear system of equations is obtained and solved by using the GMRES.
- **3**.2. The velocity is computed using Eq. (30), Eq. (31) and Eq. (32).
- **3**.3. The potential is updated to the next sub-step (ϕ_{n+1}^{k+1}) by applying the integration scheme to the kinematic relation for the free surface (Eq. (3) or Eq. (8)).
- **3**.4. The positions of the fluid particles are updated to the next sub-step ($\mathbf{x}_{n+1}^{k+1}$) using the known velocity field. If fluid particles are separated from the walls or body surface, these are relocated back to the boundaries using a normal projection.
- **3**.5. The flux is computed in the next sub-step (q_{n+1}^{k+1}) using the kinematic equations for the walls, bottom surface, and body surface.
- **3**.6. For the RK4 scheme, this process is repeated four times ($k = 1$ to $k = 4$).

4. The fluid forces on the body are computed (Eq. (35) and Eq. (34)).

5. The volume and total energy is calculated in order to monitor their temporal evolution as,

$$V(t) = \int_{\Gamma(t)} z(\boldsymbol{\lambda}_z \mathbf{n}) d\Gamma \tag{41}$$

$$e(t) = \frac{\rho g}{2} \int_{\Gamma(t)} z^2(\boldsymbol{\lambda}_z \mathbf{n}) + \phi q d\Gamma \tag{42}$$

where $\boldsymbol{\lambda}_z$ is the unit vertical vector.

6. Steps 2 to 5 are carried out iteratively until a maximum time is reached.

It should be noted that we are employing a collocational method and all variables are evaluated at the collocations points. The values of the variables on the control points can be obtained using the interpolation matrix.

5 NUMERICAL RESULTS

In this section we show some numerical examples to validate the present IGA-BEM formulation. Each example is focused on a particular computational aspect of the method. The first example is a train of small amplitude waves and we analyse the spatial convergence of the IGA-BEM solution. In the next example we simulate a solitary wave to evaluate the temporal stability and the accuracy of the method. In the third example we check the ability of the method to handle wave-structure problems by simulating the waves generated in a tank.

All geometric models were construct using the T-spline plugin of Rhino [70]. Symmetric boundary conditions were imposed at the symmetric planes of the problems. These planes have the zero flux condition as the wall and are not discretized because symmetric conditions are implicitly incorporated in the Green function. Moreover, unless otherwise is specified, the time was made dimensionless using the time scale $\sqrt{h/g}$ with h being the depth of water tank. The dimensionless variables are denoted with *.

5.1 Periodic wave: convergence of the spatial discretization

The objective of this example is to analyse the convergence of the IGA-BEM method presented in this study. The test, which has analytical solution, consists on the propagation of steady regular gravity waves over a horizontal bottom surface. For the case of small wave amplitude with respect to the depth and the wavelength λ, the dynamic boundary conditions on the free surface (Eq. (4)) can be linearised and the exact solution to potential and the free surface elevation (η) can be written as:

$$\bar{\phi}(x, z, t) = \frac{A\omega}{k} \frac{\cosh(k(z+h))}{\cosh(kh)} \sin(kx - \omega t) \tag{43}$$

$$\bar{\eta} = A\cos(kx - \omega t) \tag{44}$$

where A is the amplitude, h is the depth, ω is the wave frequency, and $k = 2\pi/\lambda$ is the wave number.

This is a 2D periodic problem where the gravity waves propagate along the x-direction and they are invariant along y-direction. Since the presented method is formulated in 3D, we study a representative domain (Ω) defined by its length $x = [0, 2\lambda]$, depth $z = [0, -\lambda]$ and width

$y = [0, 2\lambda]$. The parameters are set by the relation between the amplitude and the wave number $kA = 0.2$, and the dispersion equation $\omega^2 = gk\tanh(kh)$. Moreover, a specific time $\bar{t} = \pi/(2\omega)$ is chosen such the flux across the lateral boundaries along the longitudinal direction are zero.

Considering three symmetric planes at $x = 2\lambda$, $y = 2\lambda$ and $z = -\lambda$, the geometry is discretized with three NURBS surfaces. Note that these surfaces can be converted into a unique T-spline patch. We set a number of Bézier elements that varies in a range from 8 to 24 regular elements with an increment of 4 elements per wavelength along the longitudinal direction, while along the other two directions we utilize 24 Bézier elements. All weights are set to unity. Moreover, three different basis degree $p = 2, 3, 4$ are selected.

It should be noted that a sinusoidal function cannot be represented exactly by a rational spline, and a geometrical error is expected. To minimize this error we use a L^2-projection method. Fig. 3a shows the L^2-error between the elevation function and the free surface representation. It can be seen that the geometrical discretization shows an optimal convergence (i.e. convergence rate $\geq p + 1$). In the same line, given the potential function expressed in Eq. (43), we use the L^2-projection technique to apply the boundary conditions on the free surface. Its convergence is also optimal as shown in Fig. 3b.

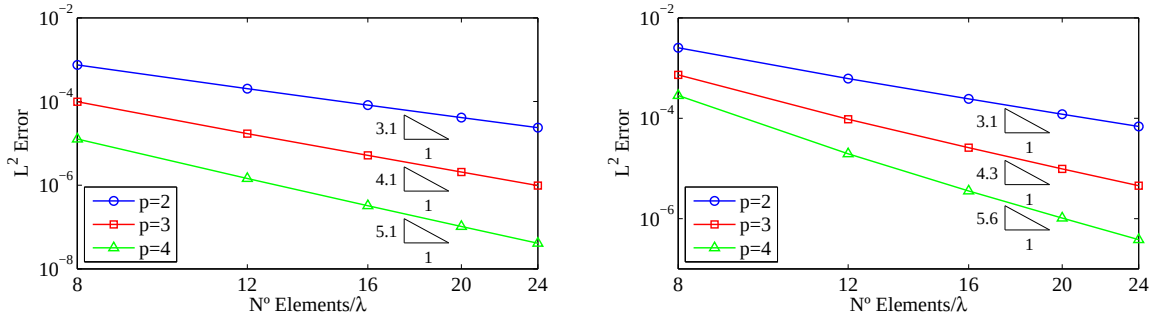

Figure 3: a) L^2-Error between the elevation function and the NURBS surface that represent the free surface in a central domain $[\lambda \times \lambda]$. b) L^2-Error between the potential function and the boundary conditions applied on the free surface in the same domain.

In Fig. 4 we show the point-wise error between the analytic and BEM solution ($\|w - w^h\|$ with w^h being the flux or potential) for three levels of refinement (8, 16 and 24 elements per wavelength) and the standard cubic basis degree. The error on the Neumann boundaries is considerable lower (one order of magnitude smaller) than on the Dirichlet boundary (free surface). Moreover, small fluctuations are detected near the intersections of the free surface due to lateral boundary effects that become negligible for a distance greater than $\lambda/2$.

Given the previous findings, we limit the converge study of the IGA-BEM solution to a central region $[\lambda \times \lambda]$ of the free surface. The result is given in Fig. 5 where an optimal convergence ratio is shown for all cases.

5.2 Solitary wave: temporal accuracy

Our next benchmark example consists on a solitary wave propagating over constant depth. This example has been studied by Tanaka [91], who obtained a 2D full non-linear numerical solution, and then used by other authors to validate their models [3,25,92]. In this subsection we

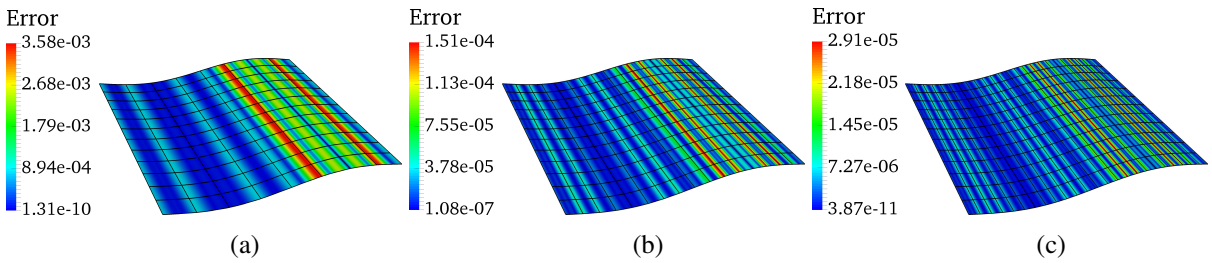

Figure 4: Point-wise error between the analytic and numeric (IGA-BEM) solution in the center region $[\lambda \times \lambda]$ of the free surface using cubic basis functions for three levels of refinement: a) 8 elements/λ, b) 16 elements/λ and c) 24 elements/λ.

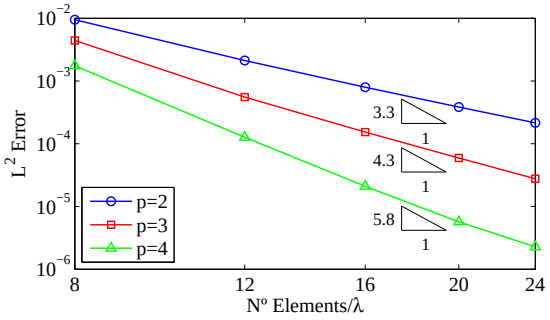

Figure 5: L^2-Error between the analytical and numerical (IGA-BEM) solution for the central domain $[\lambda \times \lambda]$ on the free surface.

analyse the temporal stability and accuracy of the present method by computing the numerical errors along the time with respect to the steady solution presented by Dutykha and Clamond [92].

We consider a wave of amplitude $A = 0.6h$, where h is the depth of the free surface at the rest. The domain is given by a length $x = [0, 20h]$, width $y = [0, 2h]$ and depth $z = [0, -h]$. The wave is propagated along the longitudinal direction (x-direction) and at the initial stage the crest is located at $x = 7.5h$.

As in the previous example, we set three symmetric planes at at $x = 20h$, $y = 2h$ and $z = -h$ and the model is represented by three NURBS surfaces with weight unity. The free surface elevation and the potential are established with the L^2-projection method applied over the solution proposed by Dutykha and Clamond [92]. We consider two longitudinal discretizations with element lengths of 0.25 and 0.5. The element length along y-direction is 0.5 and 0.25 along z-direction. We use quadratic and cubic NURBS basis functions. Moreover, simulations with an equivalent model using the standard quadratic Lagrangian basis functions has been performed for comparison purposes.

We carried out some simulations for different Courant numbers (calculated based on the length of the elements of the free surface along x-direction, given the invariance along y-direction) in the range of $0.3 \leq \mathcal{C} \leq 1.0$. The instantaneous shape, energy and volume of the wave have been monitored during a period of $\Delta t^* = 4$. We found that the wave is kept stable during the simulation for all cases and the elements are concentrated around the crest, as it can be seen in Fig.6. In Fig. 7 we show the average of the relative energy error ($\epsilon_e = (e(t) - e(0))/e(0)$), volume error ($\epsilon_v = (V(t) - V(0))/V(0)$) and L^2-error of the shape normalized by $h\sqrt{A_F}$ with A_F being the area of the free surface. It can be seen that the errors

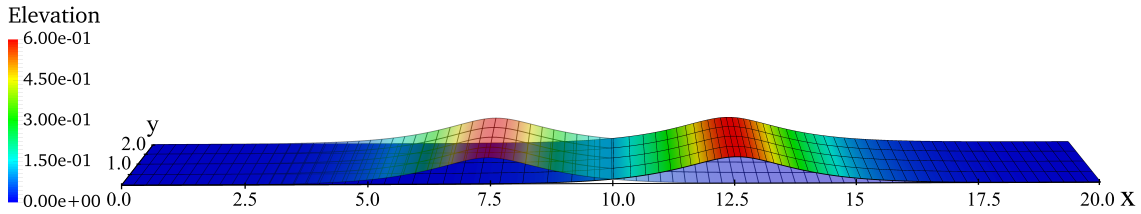

Figure 6: Time evolution of the wave shape. The translucent surface correpond to he initial condition and the solid surface to $t^* = 4$. Simulation with the fine mesh using cubic NURBS basis functions.

are mostly constant for the complete range of Courant numbers considered. This demonstrates the robustness and stability of the scheme of integration. These errors decrease as the physical discretization is finer and the basis degree increase.

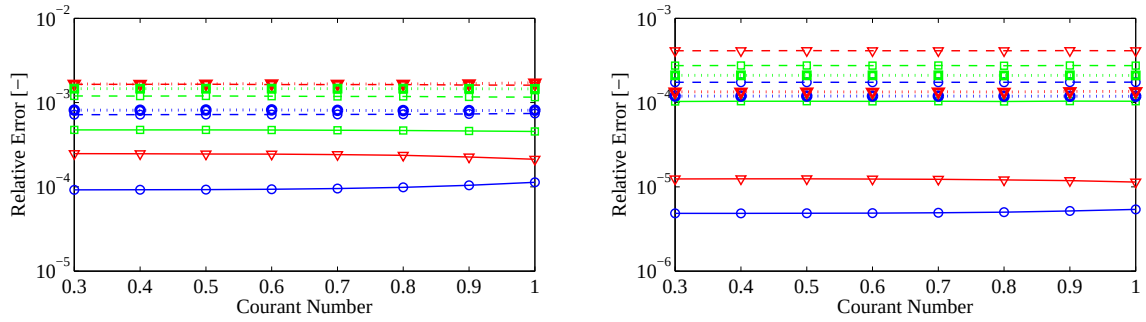

Figure 7: Relative energy (triangle), volumen (circle) and shape (square) errors for a cubic NURBS (continuouos line), quadratic NURBS (dash line) and cuadratic Lagrangian (dotted line) model, for a) the case of a coarse mesh and b) the fine mesh .

We also analysed the numerical stability of the same solitary wave propagating over a 1:15 slope that starts at the initial position of the crest ($x = 7.5h$). This configuration, that produces the overturn of the wave, was studied in detail by Grilli et al. [2] using a 2D BEM mode. Later these results have been used used to validate a 3D BEM formulation [3]. Here we consider the numerical model described above for the fine mesh and a Courant number of 0.5. Additionally, we discretize the bottom surface with the same number of uniform elements than the free surface and we extend the length of domain up to $x = 22h$. The simulation is carried out until the wave reaches the breaking point (at $t^*_{BP} = 7.78$). At larger times the lateral mesh becomes very distorted and the numerical errors increase very fast. In fact, for the quadratic Lagrange model, numerical instabilities appear before that point (at $t^* = 7.11$), as it can be observed in Fig. 8a, and the simulation stops. This problem is associated with the lack of smoothness across the elements that produces a sawtooth effect near the crest. However, the models using NURBS are stable for $t^* <= 7.78$ and the free surface remains smooth (see Fig. 8a and b). For the cubic NURBS model the wave reaches a maximum height of $6.85 \cdot 10^{-1} h$ which is very close to the reported in [2] ($6.89 \cdot 10^{-1} h$), while for the quadratic NURBS model is lightly lower ($6.81 \cdot 10^{-1} h$) due to the lower degree of accuracy. In Fig. 9 we compare the central section of the cubic NURBS model and the results presented by Grilli et al. [2] at the breaking time. The relative errors for volume and energy are $\epsilon_v = 1.21 \cdot 10^{-4}$ and $\epsilon_e = 7.62 \cdot 10^{-5}$, respectively, and the shape is in very good agreement with the data reported in [2].

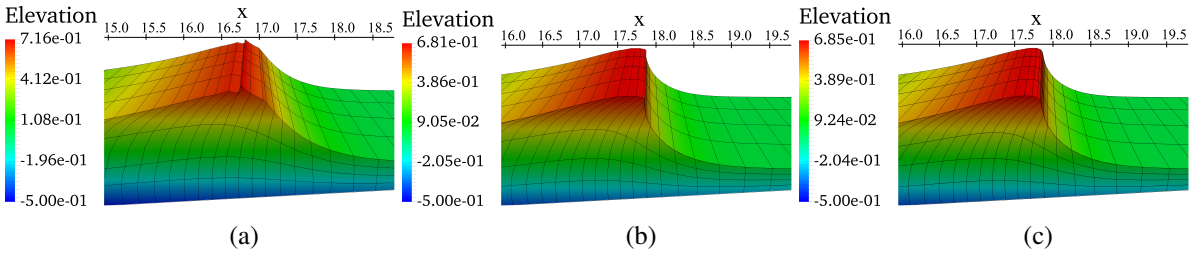

(a) (b) (c)

Figure 8: Wave shape for a) the Lagrangian model at $t^* = 7.11$, when numerical inestabilities appear, and for b) the quadratic and c) cubic NURBS models at the breaking time (at $t^* = 7.78$.)

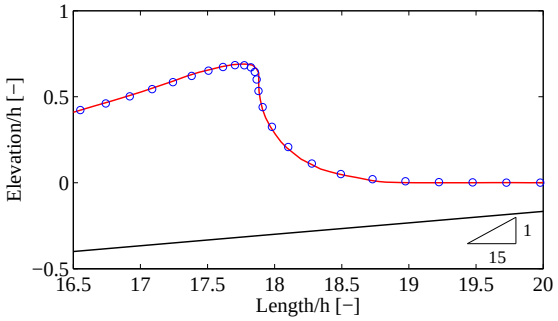

Figure 9: Wave shape of the central section (at $y = 1h$) for the present cubic NURBS model (circles) and for the results presented by Grilli et al. [2] using a 2D BEM model (continuous line) at the breaking time ($t^* = 7.78$).

5.3 Wave in a cylindrical tank: Fluid-structure interaction

The objective of this section is to demonstrate the ability of the present formulation to reproduce fluid-structure phenomenon considering the effect of the waves propagating on the free surface of a tank.

We consider a cylindrical water tank with a solid cylindrical bar located at the center. The radius of the tank is $r_T = 10h$ and the bar is $r_B = 1h$ with h being the depth of the tank. Initially a wave is established in the middle point between the the bar and the external wall of the tank. The elevation of the wave is given by a Gaussian pulse $z = Aexp[-(x - (r_B + r_T)/2)^2 - y^2]$ with $A = 0.1h$ being the amplitude of the wave. This problem has been solved by Chern et al. [93] using a Pseudo-Spectral Matrix Element Method and then used by Bai and Taylor [10] to validated their BEM formulation. More details about the problem can be found in [10, 93].

The geometry is discretized using three regular cubic NURBS surfaces that represent the free surface, the bar and the external wall. Two symmetry planes are considered at $y = 0$ and $z = -h$. We set 26×25 Bézier elements (radial $\times$ circumferential) for the free surface, and 6×25 (vertical $\times$ circumferential) for the body and external wall. There are a total of 1316 control points.

A comparison of the surface elevation adjacent to the body ($[x = r_B, y = 0]$) and horizontal force along the time between the present results and those reported by Chern et al. [93] is shown in Fig. 10. The simulation is run until $t^* = 30$ with a time step $\Delta t^* = 0.1$. As it can be seen, the present results are in good agreement with those in [93] where we have used less DoF than the required by [10] to obtain a close approximation (this is, 1316 vs 4208 DoF of the mesh b in Fig. 3a).

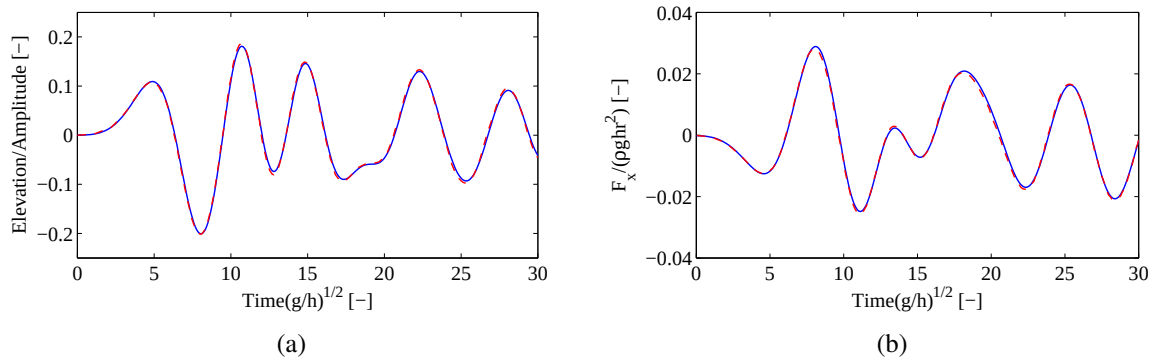

Figure 10: Time evolution of a) surface elevation adjacent to the body ($[x = r_B, y = 0]$) and b) horizontal force ($F_x/(\rho g h r^2)$). Present results: continuous line and results in [93]: dash line.

6 CONCLUSIONS

In this paper a 3D IGA-BEM formulation using T-spline and NURBS basis to study fully non-linear gravity wave propagation in the time domain has been presented. The use of splines basis provides a high geometrical approximation and also it can be directly integrated with computer aid geometrical design tools. The properties of these basis within the BEM have been analysed using numerical examples. First, an optimal spatial convergence of the method have been demonstrated simulating a periodic wave. Following, the temporal stability and accuracy have been analysed simulating the propagation of a solitary gravity wave. The numerical errors are kept practically constant to a low order over a wide range of time steps demonstrating the robustness of the time marching scheme. Moreover, the smoothness of the basis provides stability to the method without the need of artificial smooth techniques, and it allows relatively large distortion of elements. In addition, the ability of the method to the simulate the fluid-structure interaction with fixed bodies has been shown simulating the waves field in a tank.

ACKNOWLEDGMENTS

This study has been supported by the Spanish Ministerio de Economía y Competitividad under project CTQ2013-46799-C2-1-P.

REFERENCES

[1] S. T. Grilli, S. Vogelmann, P. Watts, Development of a 3d numerical wave tank for modeling tsunami generation by underwater landslides, Engineering Analysis with Boundary Elements 26 (4) (2002) 301–313.

[2] S. T. Grilli, I. A. Svendsen, R. Subramanya, Breaking criterion and characteristics for solitary waves on slopes, Journal of Waterway, Port, Coastal and Ocean Engineering 123 (3) (1997) 102–112.

[3] S. T. Grilli, P. Guyenne, F. Dias, A fully non-linear model for three-dimensional overturning waves over an arbitrary bottom, International Journal for Numerical Methods in Fluids 35 (7) (2001) 829–867.

[4] P. Guyenne, S. T. Grilli, Numerical study of three-dimensional overturning waves in shallow water, Journal of Fluid Mechanics 547 (2006) 361–388.

[5] N. Mizutani, A. M. Mostafa, K. Iwata, Nonlinear regular wave, submerged breakwater and seabed dynamic interaction, Coastal Engineering 33 (2–3) (1998) 177–202.

[6] H. K. Johnson, T. V. Karambas, I. Avgeris, B. Zanuttigh, D. Gonzalez-Marco, I. Caceres, Modelling of waves and currents around submerged breakwaters, Coastal Engineering 52 (10–11) (2005) 949–969.

[7] S. Sun, G. Wu, Fully nonlinear simulation for fluid/structure impact: A review, Journal of Marine Science and Application 13 (3) (2014) 237–244.

[8] M. Au, C. Brebbia, Diffraction of water waves for vertical cylinders using boundary elements, Applied Mathematical Modelling 7 (2) (1983) 106–114.

[9] W. Koo, M. Kim, Numerical simulation of nonlinear wave and force generated by a wedge-shape wave maker, Ocean Engineering 33 (8-9) (2006) 983–1006.

[10] W. Bai, R. Eatock Taylor, Higher-order boundary element simulation of fully nonlinear wave radiation by oscillating vertical cylinders, Applied Ocean Research 28 (4) (2006) 247–265.

[11] G. Ducrozet, F. Bonnefoy, D. L. Touzé, P. Ferrant, A modified High-Order Spectral method for wavemaker modeling in a numerical wave tank, European Journal of Mechanics - B/Fluids 34 (2012) 19 – 34.

[12] P. Ferrant, D. L. Touzé, K. Pelletier, Non-linear time-domain models for irregular wave diffraction about offshore structures, International Journal for Numerical Methods in Fluids 43 (2003) 1257–1277.

[13] S. Jeon, Y. Cho, M. Seo, J. Cho, W. Jeong, Dynamic response of floating substructure of spar-type offshore wind turbine with catenary mooring cables, Ocean Engineering 72 (2013) 356–364.

[14] T. Shivaji Ganesan, D. Sen, Time-domain simulation of large-amplitude wave–structure interactions by a 3d numerical tank approach, Journal of Ocean Engineering and Marine Energy 1 (3) (2015) 299–324.

[15] R. A. Watai, F. Ruggeri, C. M. P. Sampaio, A. N. Simos, Development of a time domain boundary element method for numerical analysis of floating bodies' responses in waves, Journal of the Brazilian Society of Mechanical Sciences and Engineering 37 (5) (2015) 1569–1589.

[16] W. Koo, M. Kim, D. Lee, S. Hong., Nonlinear time-domain simulation of pneumatic floating breakwater, International Journal of Offshore and Polar Engineering 16 (1) (2006) 25–32.

[17] M. S. Longuet-Higgins, E. D. Cokelet, The deformation of steep surface waves on water. i. a numerical method of computation, Proceedings of the Royal Society of London A: Mathematical, Physical and Engineering Sciences 350 (1660) (1976) 1–26.

[18] T. Nakayama, K. Washizu, The boundary element method applied to the analysis of two-dimensional nonlinear sloshing problems, International Journal for Numerical Methods in Engineering 17 (11) (1981) 1631–1646.

[19] T. Nakayama, Boundary element analysis of nonlinear water wave problems, International Journal for Numerical Methods in Engineering 19 (7) (1983) 953–970.

[20] D. Skyner, A comparison of numerical predictions and experimental measurements of the internal kinematics of a deep-water plunging wave, Journal of Fluid Mechanics 315 (1996) 51–64.

[21] S. Maiti, D. Sen, Computation of solitary waves during propagation and runup on a slope, Ocean Engineering 26 (11) (1999) 1063–1083.

[22] M. Abou-Dina, M. Helal, Boundary integral method applied to the transient, nonlinear wave propagation in a fluid with initial free surface elevation, Applied Mathematical Modelling 24 (8–9) (2000) 535–549.

[23] D. G. Dommermuth, D. K. P. Yue, W. M. Lin, R. J. Rapp, E. S. Chan, W. K. Melville, Deep-water plunging breakers: a comparison between potential theory and experiments, Journal of Fluid Mechanics 189 (1988) 423–442.

[24] S. T. Grilli, J. Skourup, I. Svendsen, An efficient boundary element method for nonlinear water waves, Engineering Analysis with Boundary Elements 6 (2) (1989) 97–107.

[25] S. T. Grilli, I. A. Svendsen, Corner problems and global accuracy in the boundary element solution of nonlinear wave flows, Engineering Analysis with Boundary Elements 7 (4) (1990) 178–195.

[26] K. Tanizawa, The state of the art on numerical wave tank, Proceedings of the 4th Osaka Colloquium on seakeeping performance of ships (2000) 95–114.

[27] C. C. Lee, Y. H. Liu, C. H. Kim, Simulation of nonlinear waves and forces due to transient and steady motion of submerged sphere, International Journal of Offshore and Polar Engineering 416 (1994) 174–182.

[28] W. Bai, R. E. Taylor, Numerical simulation of fully nonlinear regular and focused wave diffraction around a vertical cylinder using domain decomposition, Applied Ocean Research 29 (1–2) (2007) 55–71.

[29] W. Bai, R. E. Taylor, Fully nonlinear simulation of wave interaction with fixed and floating flared structures, Ocean Engineering 36 (3–4) (2009) 223–236.

[30] H. G. Sung, S. T. Grilli, BEM Computations of 3-D Fully Nonlinear Free-Surface Flows Caused by Advancing Surface Disturbances, International Journal of Offshore and Polar Engineerin 18 (2008) 292–301.

[31] M. Hannan, W. Bai, K. Ang, Modeling of fully nonlinear wave radiation by submerged moving structures using the higher order boundary element method, Journal of Marine Science and Application 13 (1) (2014) 1–10.

[32] W. Bai, M. Hannan, K. Ang, Numerical simulation of fully nonlinear wave interaction with submerged structures: Fixed or subjected to constrained motion, Journal of Fluids and Structures 49 (2014) 534–553.

[33] E. Dombre, M. Benoit, D. Violeau, C. Peyrard, S. T. Grilli, Simulation of floating structure dynamics in waves by implicit coupling of a fully non-linear potential flow model and a rigid body motion approach, Journal of Ocean Engineering and Marine Energy 1 (1) (2014) 55–76.

[34] E. Guerber, M. Benoit, S. T. Grilli, C. Buvat, A fully nonlinear implicit model for wave interactions with submerged structures in forced or free motion, Engineering Analysis with Boundary Elements 36 (2012) 1151–1163.

[35] G. Chen, C. Kharif, S. Zaleski, J. Li, Two-dimensional Navier–Stokes simulation of breaking waves, Physics of Fluids 11 (1) (1999) 121–133.

[36] S. Guignard, R. Marcer, V. Rey, C. Kharif, P. Fraunié, Solitary wave breaking on sloping beaches: 2-D two phase flow numerical simulation by SL-VOF method, European Journal of Mechanics - B/Fluids 20 (1) (2001) 57–74.

[37] I. Hadžić, J. Hennig, M. Perić, Y. Xing-Kaeding, Computation of flow-induced motion of floating bodies, Applied Mathematical Modelling 29 (12) (2005) 1196–1210.

[38] M. A. Rahman, N. Mizutani, K. Kawasaki, Numerical modeling of dynamic responses and mooring forces of submerged floating breakwater, Coastal Engineering 53 (10) (2006) 799–815.

[39] Y. Li, M. Lin, Regular and irregular wave impacts on floating body, Ocean Engineering 42 (2012) 93–101.

[40] A. Ghasemi, A. Pathak, M. Raessi, Computational simulation of the interactions between moving rigid bodies and incompressible two-fluid flows, Computers & Fluids 94 (2014) 1–13.

[41] M. Okan, S. Umpleby, Free surface flow around arbitrary two-dimensional bodies by b-splines, International Shipbuilding Progress 32 (372) (1985) 182–187.

[42] D. Kring, P. Sclavounos, Numerical stability analysis for time-domain ship motion simulations, Journal of Ship Research 39 (4) (1995) 313–320.

[43] T. Peltzer, B. Rosenthal, W. Reppun, D. Kring, W. Milewski, B. Connell, Multi-body seakeeping design optimization, Proc. Eighth Int. Conf. Hydrodyn. (ICHD2008).

[44] B. Kim, Y. Shin, A NURBS Panel Method for Three-dimensional Radiation and Diffraction Problems, Journal of Ship Research 47 (2) (2003) 177–186.

[45] G.-D. Kim, C.-S. Lee, J. Kerwin, A B-spline based higher order panel method for analysis of steady flow around marine propellers, Ocean Engineering 34 (14-15) (2007) 2045–2060.

[46] Z. Gao, Z. Zou, A NURBS-based high-order panel method for three-dimensional radiation and diffraction problems with forward speed, Ocean Engineering 35 (11-12) (2008) 1271–1282.

[47] T. Hughes, J. Cottrell, Y. Bazilevs, Isogeometric analysis: CAD, finite elements, NURBS, exact geometry and mesh refinement, Computer Methods in Applied Mechanics and Engineering 194 (39–41) (2005) 4135–4195.

[48] T. Hughes, Isogeometric analysis: Progress and challenges, Conference on Mathematical Methods for Curves & Surfaces (MMCS'08), 2008.

[49] J. Cottrell, T. Hughes, A. Reali, Studies of refinement and continuity in isogeometric structural analysis, Computer Methods in Applied Mechanics and Engineering 196 (41-44) (2007) 4160–4183.

[50] J. Cottrell, T. Hughes, Y. Bazilevs, Isogeometric Analysis: Toward Integration of CAD and FEA, John Wiley & Sons, 2009.

[51] C. Politis, A. Ginnis, P. Kaklis, K. Belibassakis, C. Feurer, An isogeometric BEM for exterior potential-flow problems in the plane, 2009, pp. 349–354.

[52] R. Simpson, S. Bordas, J. Trevelyan, T. Rabczuk, A two-dimensional isogeometric boundary element method for elastostatic analysis, Computer Methods in Applied Mechanics and Engineering 209-212 (2012) 87–100.

[53] K. Belibassakis, T. Gerostathis, K. Kostas, C. Politis, P. Kaklis, A. Ginnis, C. Feurer, A BEM-isogeometric method for the ship wave-resistance problem, Ocean Engineering 60 (2013) 53–67.

[54] T. Sederberg, J. Zheng, A. Bakenov, A. Nasri, T-splines and T-NURCCs, Vol. 22, 2003, pp. 477–484.

[55] M. Scott, X. Li, T. Sederberg, T. Hughes, Local refinement of analysis-suitable T-splines, Computer Methods in Applied Mechanics and Engineering 213-216 (2012) 206–222.

[56] X. Li, J. Zheng, T. W. Sederberg, T. J. Hughes, M. A. Scott, On linear independence of T-spline blending functions, Computer Aided Geometric Design 29 (1) (2012) 63–76.

[57] M. Borden, M. Scott, J. Evans, T. Hughes, Isogeometric finite element data structures based on Bézier extraction of NURBS, International Journal for Numerical Methods in Engineering 87 (1-5) (2011) 15–47.

[58] M. Scott, R. Simpson, J. Evans, S. Lipton, S. Bordas, T. Hughes, T. Sederberg, Isogeometric boundary element analysis using unstructured T-splines, Computer Methods in Applied Mechanics and Engineering 254 (0) (2013) 197–221.

[59] D. Thomas, M. Scott, J. Evans, K. Tew, E. Evans, Bézier projection: A unified approach for local projection and quadrature-free refinement and coarsening of NURBS and T-splines with particular application to isogeometric design and analysis, Computer Methods in Applied Mechanics and Engineering 284 (2015) 55–105.

[60] D. Benson, Y. Bazilevs, M.-C. Hsu, T. Hughes, A large deformation, rotation-free, isogeometric shell, Computer Methods in Applied Mechanics and Engineering 200 (13-16) (2011) 1367–1378.

[61] C. Verhoosel, M. Scott, T. Hughes, R. de Borst, An isogeometric analysis approach to gradient damage models, International Journal for Numerical Methods in Engineering 86 (1) (2011) 115–134.

[62] C. Verhoosel, M. Scott, R. De Borst, T. Hughes, An isogeometric approach to cohesive zone modeling, International Journal for Numerical Methods in Engineering 87 (1-5) (2011) 336–360.

[63] D. Schillinger, L. Dedè, M. Scott, J. Evans, M. Borden, E. Rank, T. Hughes, An isogeometric design-through-analysis methodology based on adaptive hierarchical refinement of NURBS, immersed boundary methods, and T-spline CAD surfaces, Computer Methods in Applied Mechanics and Engineering 249-252 (2012) 116–150.

[64] Z. Kacprzyk, K. Ostapska-Luczkowska, Isogeometric analysis as a new fem formulation-simple problems of steady state thermal analysis, Procedia Engineering 91 (2014) 87–92.

[65] R. Simpson, M. Scott, M. Taus, D. Thomas, H. Lian, Acoustic isogeometric boundary element analysis, Computer Methods in Applied Mechanics and Engineering 269 (2014) 265–290.

[66] A. Ginnis, K. Kostas, C. Politis, P. Kaklis, K. Belibassakis, T. Gerostathis, M. Scott, T. Hughes, Isogeometric boundary-element analysis for the wave-resistance problem using T-splines, Computer Methods in Applied Mechanics and Engineering 279 (0) (2014) 425–439.

[67] K. Kostas, A. Ginnis, C. Politis, P. Kaklis, Ship-hull shape optimization with a T-spline based BEM-isogeometric solver, Computer Methods in Applied Mechanics and Engineering 284 (2015) 611–622.

[68] V. Nguyen, C. Anitescu, S. Bordas, T. Rabczuk, Isogeometric analysis: An overview and computer implementation aspects, Mathematics and Computers in Simulation 117 (2015) 89–116.

[69] S. Lipton, J. Evans, Y. Bazilevs, T. Elguedj, T. Hughes, Robustness of isogeometric structural discretizations under severe mesh distortion, Computer Methods in Applied Mechanics and Engineering 199 (5–8) (2010) 357–373.

[70] T-splines, inc, http://www.tsplines.com.

[71] H. G. Sung, H. S. Choi, Implicit formulation with the boundary element method for nonlinear radiation of water waves, Engineering Analysis with Boundary Elements 34 (5) (2010) 511–529.

[72] L. Piegls, W. Tiller, The NURBS Book, 2nd Edition, Springer, 1996.

[73] Y. Bazilevs, V. Calo, J. Cottrell, J. Evans, T. Hughes, S. Lipton, M. Scott, T. Sederberg, Isogeometric analysis using T-splines, Computer Methods in Applied Mechanics and Engineering 199 (5-8) (2010) 229–263.

[74] E. Evans, M. Scott, X. Li, D. Thomas, Hierarchical T-splines: Analysis-suitability, Bézier extraction, and application as an adaptive basis for isogeometric analysis, Computer Methods in Applied Mechanics and Engineering 284 (2014) 1–20.

[75] X. Li, Some properties for analysis-suitable T-splines, Journal of Computational Mathematics 33 (4) (2015) 428–442.

[76] V. Mantic, A new formula for the C-matrix in the Somigliana identity, Journal of Elasticity 33 (3) (1993) 191–201.

[77] M. Scott, M. Borden, C. Verhoosel, T. Sederberg, T. Hughes, Isogeometric finite element data structures based on Bézier extraction of T-splines, International Journal for Numerical Methods in Engineering 88 (2) (2011) 126–156.

[78] C. A. Brebbia, J. Domínguez, Boundary Elements: An Introductory Course, second edition Edition, WIT Press, Computational Mechanics, 1992.

[79] J. Lachat, J. Watson, Effective numerical treatment of boundary integral equations: A formulation for three-dimensional elastostatics, International Journal for Numerical Methods in Engineering 10 (5) (1976) 991–1005.

[80] C. Adam, T. Hughes, S. Bouabdallah, M. Zarroug, H. Maitournam, Selective and reduced numerical integrations for NURBS-based isogeometric analysis, Computer Methods in Applied Mechanics and Engineering 284 (2015) 732–761.

[81] G. Xie, J. Zhang, Y. Dong, C. Huang, G. Li, An improved exponential transformation for nearly singular boundary element integrals in elasticity problems, International Journal of Solids and Structures 51 (6) (2014) 1322–1329.

[82] G. Xie, F. Zhou, J. Zhang, X. Zheng, C. Huang, New variable transformations for evaluating nearly singular integrals in 3d boundary element method, Engineering Analysis with Boundary Elements 37 (9) (2013) 1169–1178.

[83] B. I. Yun, A generalized non-linear transformation for evaluating singular integrals, International Journal for Numerical Methods in Engineering 65 (12) (2006) 1947–1969.

[84] J. Telles, R. Oliveira, Third degree polynomial transformation for boundary element integrals: Further improvements, Engineering Analysis with Boundary Elements 13 (2) (1994) 135–141.

[85] X.-W. Gao, The radial integration method for evaluation of domain integrals with boundary-only discretization, Engineering Analysis with Boundary Elements 26 (10) (2002) 905–916.

[86] X.-W. Gao, An effective method for numerical evaluation of general 2d and 3d high order singular boundary integrals, Computer Methods in Applied Mechanics and Engineering 199 (45–48) (2010) 2856–2864.

[87] J. C. F. Telles, A self-adaptive co-ordinate transformation for efficient numerical evaluation of general boundary element integrals, International Journal for Numerical Methods in Engineering 24 (5) (1987) 959–973.

[88] A. Brancati, M. Aliabadi, I. Benedetti, Hierarchical adaptive cross approximation gmres technique for solution of acoustic problems using the boundary element method, Computer Modeling in Engineering and Sciences 43 (2) (2009) 149–172.

[89] G. Wu, R. Taylor, The coupled finite element and boundary element analysis of nonlinear interactions between waves and bodies, Ocean Engineering 30 (3) (2003) 387–400.

[90] S. Boo, C. Kim, Fully nonlinear diffraction due to a vertical circular cylinder in a 3-D HOBEM numerical wave tank, Proceedings of the International Offshore and Polar Engineering Conference 3 (1996) 23–30.

[91] M. Tanaka, The stability of solitary waves, Physics of Fluids 29 (3) (1986) 650–655.

[92] D. Dutykh, D. Clamond, Efficient computation of steady solitary gravity waves, Wave Motion 51 (1) (2014) 86–99.

[93] M. Chern, A. Borthwick, R. Taylor, Simulation of non-linear free surface motions in a cylindrical domain using a chebyshev-fourier spectral collocation method, International Journal for Numerical Methods in Fluids 36 (4) (2001) 465–496.

[94] P. Ferrant, A coupled time and frequency approach for nonlinear wave radiation, In Eighteenth Symposium on Naval Hydrodynamics (1991) 67–83.